micro

MDPI

Article

Preparation, Characterization, and Acetylcholinesterase Inhibitory Ability of the Inclusion Complex of β-Cyclodextrin–Cedar (*Juniperus phoenicea*) Essential Oil

Eleni Kavetsou [1], Ioanna Pitterou [1], Annita Katopodi [1], Georgia Petridou [1], Abdelaziz Adjali [2], Spyros Grigorakis [2] and Anastasia Detsi [1,*]

[1] Laboratory of Organic Chemistry, School of Chemical Engineering, National Technical University of Athens, 15780 Athens, Greece; ekavetsou@central.ntua.gr (E.K.); ipitterou@gmail.com (I.P.); annitakatopodi@mail.ntua.gr (A.K.); georgiapetridou_@outlook.com (G.P.)

[2] Department of Food Quality and Chemistry of Natural Products, Mediterranean Agronomic Institute of Chania (Centre International de Hautes Etudes Agronomiques Mediterraneennes), 73100 Crete, Greece; Aadjali@maich.gr (A.A.); grigorakis@maich.gr (S.G.)

* Correspondence: adetsi@chemeng.ntua.gr

Abstract: The aim of the present study was the encapsulation of cedar (*Juniperus phoenicea*) essential oil (CEO) of Greek origin in β-cyclodextrin (β-CD) through the formation of inclusion complexes (ICs) using the co-precipitation method with different β-CD-to-CEO weight ratios (90:10, 85:15, 80:20, 70:30 (*w*/*w*)). The encapsulation of CEO in β-CD through host–guest interactions was confirmed by Nuclear Magnetic Resonance (NMR) spectroscopy, FT-IR spectroscopy, Differential Scanning Calorimetry (DSC) and Thermogravimetric Analysis (TGA). The obtained ICs exhibited nanoscale size (315.9 nm to 769.6 nm),Polydispersity Index from 0.326 to 0.604 and satisfactory stability in suspension (−37.0 mV to −17.0 mV). The process yield was satisfactory, ranging between 65% and 78%, while the inclusion efficiency ranged from 10% to 27%. The in vitro release study conducted for the IC with the optimal characteristics (β-CD:CEO 80:20 (*w*/*w*)) exhibited a sustained release profile, with an initial burst effect in the first 5 h. The release profile could be well expressed by the Higuchi equation: $Q = 18.893\ t^{1/2} + 9.5919$, $R^2 = 0.8491$. The cedar EO presented significant acetylcholinesterase inhibition (IC_{50} 37 μg/mL), which was prolonged by its encapsulation into the β-CD cavity.

Keywords: cedar (*Juniperus phoenicea*) essential oil; encapsulation; inclusion complexes; β-cyclodextrin; phase solubility studies; release profile; kinetic modeling; acetylcholinesterase inhibition

Citation: Kavetsou, E.; Pitterou, I.; Katopodi, A.; Petridou, G.; Adjali, A.; Grigorakis, S.; Detsi, A. Preparation, Characterization, and Acetylcholinesterase Inhibitory Ability of the Inclusion Complex of β-Cyclodextrin–Cedar (*Juniperus phoenicea*) Essential Oil. *Micro* **2021**, *1*, 250–266. https://doi.org/10.3390/micro1020019

Academic Editor: Nurettin Sahiner

Received: 30 September 2021
Accepted: 3 December 2021
Published: 8 December 2021

1. Introduction

Over the last few decades, there has been a growing interest in the therapeutic potential of natural products, such as essential oils (EOs), which present a wide range of biological properties, including antimicrobial [1], antioxidant [2], antivirus [3], anticancer [4] and neuroprotective [5] activities. Thereafter, EOs have found a considerable range of applications as naturally occurring bioactive agents in the field of medicine, food and cosmetic preservation [6]. The biological activities of EOs are assigned to several small molecules, including terpenoids, phenolic and aliphatic constituents. It is important to note that the place of origin of the EO, the climatic conditions, as well as the part of the plant and the method used for its extraction, significantly affect its composition and therefore its biological activities [7].

Essential oils are well known for their ability to scavenge free radicals [8], as well as to inhibit acetylcholinesterase activity [9] and suppress Aβ peptide deposits [10]. Acetylcholinesterase (AChE) is a type-B carboxylesterase that catalyzes the hydrolysis of the neurotransmitter acetylcholine in choline and acetic acid [11]. AChE inhibitors are a constantly developing research field since they comprise the main therapeutic strategy for

Alzheimer's Disease (AD) presently. Specifically, the decrease in acetylcholine levels is of major importance for the decline of the cognitive function of AD patients [12], while some of the most well-known AChE inhibitors are natural products, such as galantamine and phytostigmine. Therefore, several plant species (e.g., essential oils) producing a wide arrow of bioactive compounds, such as alkaloids, coumarins, terpenes, flavonoids and polyphenols, have been examined for their AChE inhibitory activity in the research of potential anti-AD drugs with fewer side effects [13,14].

Eos of plant species belonging to Cupressaceae family, primarily from the genera *Juniperus* and *Cupressus*, are reported to display potent biological activities. *Juniperus phoenicea,* also known as cedar, is a coniferous tree and is considered an important medicinal plant largely used in traditional medicine. Its range covers the whole Mediterranean region, from the Canary Islands, the Atlas Mountains in Africa and the Atlantic coast of Portugal in the West to Jordan and Saudi Arabia in the East [15]. Its properties are mainly based on its chemical composition, containing monoterpenes, such as α-pinene, myrcene and δ-3-carene as major constituents [16,17]. The cedar *(J. phoenicea)* essential oil (CEO) is known to possess inherent properties, including antimicrobial [17], antioxidant [18], anti-inflammatory [19] and neuroprotective, also expressed by its ability to inhibit AChE activity. For instance, *Juniperus phoenicea* EO derived using different solvents from the berries of the plant collected from Turkey presented 75% inhibition at 200 μg/mL [20].

Despite the multiple biological responses of the CEO, there is a challenging problem concerning its use in a final product due to its volatility, hydrophobic nature and sensitivity in the presence of light, oxygen and heat [21]. A common approach to overcome these limitations is nano- and microencapsulation, which is widely considered as a viable, promising and efficient technique for the development of new functional pharmaceutical, cosmetic, etc., products [22]. So far, several nanoencapsulation strategies have been developed for the delivery of natural compounds using various biodegradable carriers [23]. In fact, the encapsulation of EOs in different carriers has already been proven effective in enhancing their biological activity [24,25]. Among various methods for maintaining the quality of the EO and improving its physicochemical (e.g., aqueous solubility) and biological properties, complexation with natural and chemically modified cyclodextrins was found to be a successful strategy [26].

Cyclodextrins (CDs) are cyclic oligosaccharides consisting of six (α-cyclodextrin), seven (β-cyclodextrin) and eight (γ-cyclodextrin) d-(+)-glucopyranose units linked by α-D-(1→4) linkages. The structure of cyclodextrin molecules resembles truncated cones with the secondary hydroxyl groups located at the wider edge of the ring and the primary groups on the narrower edge. Hydrogen atoms are directed to the inner part of the ring, resulting in a hydrophobic cavity along with a hydrophilic character outside of the ring. Hence, cyclodextrins are soluble in water and simultaneously may accommodate a broad range of hydrophobic bioactive species inside their cavity through the formation of host–guest inclusion complexes (ICs) [27,28]. Several EOs have been reported to form supermolecular inclusion complexes with β-CD, such as oregano [29] and eucalyptus [30] essential oils. The complexation of EOs with β-CD increases their aqueous solubility and thermal stability (heat-promoted decomposition in higher temperatures), offers their controlled release [30] and maintains or enhances their bioactivity [31].

However, to our knowledge, there are no reports that have examined the formation of inclusion complexes of Cedar essential oil derived from a Greek region with β-cyclodextrin, along with their ability to inhibit acetylcholinesterase in vitro. The present study focuses on the encapsulation of the CEO in β-CD and the characterization of the novel inclusion complexes concerning their thermal and physicochemical properties. The in vitro release profile and the kinetic modeling were studied, as well as the effect of the β-cyclodextrin concentration in the aqueous solubility of cedar essential oil. The overall goal of this research is to propose a new method for the efficient encapsulation of the CEO and to demonstrate its feasibility in inhibiting acetylcholinesterase activity effectively.

2. Materials and Methods

2.1. Materials

Cedar *(Juniperus phoenicea)* essential oil of food-grade quality, obtained by steam distillation from the berries of *J. phoenicea*, which were collected from Viotia, Greece, during the summer of 2017, was kindly provided by the Laboratory of Nutritional Physiology and Feeding, Animal Sciences and Aquaculture Faculty, Agricultural University of Athens (A.U.A., Athens, Greece). β-Cyclodextrin (β-CD) of >99% purity was purchased from Fluka (Gillingham, England), while ethanol of analytical reagent grade, ethyl acetate, hexane, K_2HPO_4 and KH_2PO_4 of ACS grade and anhydrous sodium sulfate were purchased from Merck Millipore (Billerica, MA, USA). Acetylcholinesterase from *Electrophorus electricus*, type VI-S (Saint Louis, MO, USA), and trizma-base 99% were purchased from Merck Millipore (Billerica, MA, USA). Acetylthiocholine iodide 98%, 5,5′-dithiobis-(2-nitrobenzoic acid) 99%, Galantamine hydrobromide 98% and Dimethyl sulfoxide (DMSO) 99.8% were purchased from Alfa Aesar (Haverhill, MA, USA). The materials were used without further purification. For the preparation of solutions, ultra-pure water was used.

2.2. Chemical Analysis of CEO

The CEO was analyzed using a GC-MS VARIAN 450 GC hyphenated with a VARIAN 220 MS IT Mass Spectrometer. The method of ionization was Electron Impact, and mass analysis was performed using Ion Trap. The FactorFour capillary column (VF-5 ms; 30 m × 0.25 mm I.D.; DF = 0.25) was used, and helium was the carrier gas at a flow rate of 1.0 mL/min. The column temperature was initially kept at 36 °C and then gradually increased to 190 °C at a 3 °C min^{-1}. The mass range was recorded from *m/z* 40 to 650. The injection port temperature was at 250 °C. The samples of CEO were appropriately diluted in hexane and injected manually in the split mode (split ratio: 1:50).

2.3. Preparation of β-CD–CEO Inclusion Complexes

The β-CD–CEO ICs were prepared by the co-precipitation method [29]. Different batches of inclusion complexes (ICs) were prepared by varying the CEO-to-β-CD mass ratio. Briefly, β-CD was dissolved in defined volumes of an ethanol and double-deionized water mixture (1:2 *v*/*v*) to achieve a concentration of 100 mg/mL. The solution was magnetically stirred at 55 ± 0.5 °C until the complete dissolution of β-CD. Subsequently, the defined mass of CEO was added dropwise in the β-CD solution to obtain the determined β-CD:CEO mass ratio each time (90:10, 85:15, 80:20, 70:30 (*w*/*w*)). The formed emulsion was continuously stirred at room temperature for 24 h until the β-CD–CEO ICs were formed. The final dispersion was kept in the refrigerator for 24 h, after which the β-CD–CEO ICs were recovered by vacuum filtration. The recovered ICs were dried in a high-pressure Edward's pump for 4 h and were stored in the refrigerator for further analysis and characterization.

The process yield was determined using Equation (1):

$$\text{Process yield } (\%) = \frac{\textit{mass of recovered dried ICs}}{(\textit{initial mass of } \beta - \text{CD} + \text{initial mass of EO})} \times 100 \quad (1)$$

2.4. Characterization of the β-CD–CEO ICs

2.4.1. Inclusion Efficiency of the β-CD–CEO ICs

The inclusion efficiency (%IE) of cedar essential oil in the β-CD–CEO ICs was measured directly by quantification of the encapsulated EO in the final dried ICs via Ultraviolet-Visible Spectroscopy using a JASCO double-beam V-770 UV-Vis/NIR spectrophotometer. For the analyses, 50 mg of dried ICs were dispersed in 4 mL of double-deionized water and 2 mL of hexane. The dispersion was sonicated at 80 °C for 20 min. The organic phase was separated from the aqueous phase and then was dried using anhydrous sodium sulfate. Subsequently, the hexane was evaporated from the organic phase using a rotary evaporator

at room temperature for 30 min. Ethyl acetate was then added, and the absorption of the EO was measured at 252 nm. The IE (%) was calculated using the following Equation (2):

$$IE\ (\%) = 100 \times \frac{mass\ of\ the\ encapsulated\ \ CEO}{initial\ CEO\ mass\ to\ be\ encapsulated} \quad (2)$$

2.4.2. Determination of Size, Size Distribution and Zeta-Potential

Dynamic Light Scattering (DLS) using a Zetasizer Nano ZS device (Malvern Instruments, Malvern, UK) was utilized to measure the size, size distribution and zeta-potential of the ICs. For the DLS measurements, aqueous solutions (pH 7.0) of the final dried β-CD–CEO ICs were adequately diluted. The samples were placed in a folded capillary cell (DTS1070, Malvern, UK). The size, polydispersity index (PDI) and zeta-potential measurements were carried out in triplicate at 25 ± 1 °C. The results were reported as mean ± standard deviation (SD).

2.4.3. Thermal Properties

The thermal properties of the ICs (β-CD:CEO = 80:20 (*w*/*w*)) were studied using the Differential Scanning Calorimetry (DSC) method (DSC 1 STAR^e System device, Mettler Toledo, Columbus, OH, USA), and the Thermogravimetric (TG) analysis (TGA/DSC 1 STAR^e System Thermobalance, Mettler Toledo, Columbus, OH, USA). Both analyses were conducted for the pure β-CD, CEO and for the final dried β-CD–CEO ICs. For the DSC analyses, the samples were heated from 30 °C to 300 °C, with a heating rate of 10 °C/min under nitrogen gas flow (20 mL/min), while for the Thermogravimetric (TG) analyses, they were heated from 25 °C to 600 °C, at a heating rate of 10 °C/min under nitrogen gas flow (10 mL/min).

2.4.4. Fourier Transform Infrared Spectroscopy (FT-IR Spectroscopy)

The FT-IR-ATR spectra of the CEO, free β-CD and the β-CD–CEO ICs (β-CD:CEO = 80:20 (*w*/*w*)) were obtained using a JASCO FT/IR-4200 spectrometer (Japan Spectroscopic Company, Tokyo, Japan). IR analyses were carried out in the scanning range of 500–4000 cm^{-1}.

2.4.5. Nuclear Magnetic Resonance Spectroscopy (NMR Spectroscopy)

NMR spectrometry was used to confirm the formation of inclusion complexes. The ^{1}H-NMR spectra of the final dried β-CD–CEO ICs (β-CD:CEO = 80:20 (*w*/*w*)) and β-CD were recorded on theVarian 300 MHz spectrometer (Varian, Palo Alto, CA, USA) of the Institute of Chemical Biology of National Hellenic Research Foundation. The spectra were obtained using deuterium oxide (D_2O) as a solvent. The coupling constants (*J*) are expressed in hertz (Hz), and the chemical shifts (δ) are reported in parts per million (ppm) relative to the solvent.

2.5. Phase Solubility Studies

The phase solubility studies were conducted to investigate the effect of β-CD on the solubility of the cedar essential oil (CEO). An excess amount of the cedar essential oil (15 g/L) was added in an aqueous buffer (pH 7.4) containing increasing amounts of β-CD (ranging from 0 to 10 mmol/L) at 37 °C. The amount of cedar essential oil in suspension after equilibration for 72 h and filtration through a 0.45 μm membrane filter was determined by ultraviolet-to-visible (UV-Vis) spectroscopy [32–34].

2.6. In Vitro Release Study of the β-CD–Cedar Essential Oil (CEO) ICs

The release profile of the β-CD–Cedar Essential Oil (CEO) IC (β-CD:CEO = 80:20 (*w*/*w*)) was studied in phosphate-buffered solution (pH 7.4) at 37 °C. In particular, the release rate of CEO from β-CD–CEO ICs was carried out by adding 200 mg of β-CD–CEO ICs into 30 mL of phosphate-buffered solution (pH 7.4) and was kept under magnetic

stirring (400 rpm) for 24 h. At specific time intervals, 2 mL samples were manually withdrawn from the dissolution medium and replaced with a fresh medium to maintain a constant volume. The accumulated release amount of CEO from β-CD–CEO ICs was measured using UV-vis spectroscopy. The obtained release data were further analyzed by kinetic studies according to zero order, first order, second order, Higuchi and Korsmeyer-Peppas models. The selection of the most appropriate model was based on the obtained R^2 values [35].

2.7. In Vitro Acetylcholinesterase Inhibition Assay

Inhibition of AChE activity was assessed using a modified 96-well microplate assay [36], based on Ellman's method [37]. Specifically, thiocholine, which is the product of acetylthiocholine (ATCI) hydrolysis by AChE, reacts with Ellman's reagent (DTNB) to produce 2-nitrobenzoate-5-mercaptothiocholine and 5-thio-2-nitrobenzoate, which can be detected at 412 nm.

For free CEO, β-CD or galantamine hydrobromide, Tris-HCl 50 mM pH 8.0, each sample dissolved in DMSO and 0.1 units/mL of *electrophorus electricus* AChE was added in each well and incubated for 15 min. Then DTNB (3 mM) was added, as well as ATCI (14 mM), which initiated the reaction. Absorbance was measured at t = 0 and t = 10 min after substrate's addition at 412 nm. The percentage of inhibition was calculated by comparing the difference of absorbance's values for the sample and the control (DMSO), using the following Equation (3):

$$\%Inhibition = \left(1 - \frac{Asample_{t=10min} - Asample_{t=0min}}{Acontrol_{t=10min} - Acontrol_{t=0min}}\right) \times 100 \quad (3)$$

For the β-CD–CEO ICs (β-CD:CEO = 80:20 (w/w)), Tris-HCl 50 mM pH 8.0 and β-CD–CEO ICs dispersed in ultra-pure water or DMSO were added in each well, while *electrophorus electricus* AChE (0.1 units/mL) was added either instantly or after 2 h, 5 h and 24 h and incubated for 15 min. All the other proceedings were the same as described for free CEO inhibitory activity, while the control mixture contained water or DMSO, respectively. The IC_{50} values were calculated using the GraphPad Prism software (v. 8.0.2.) by non-linear regression.

3. Results and Discussion

3.1. Chemical Analysis of CEO

GC-MS analysis was carried out in order to determine the chemical composition of CEO. In total, seven compounds were identified, making up 92.6% of the CEO. CEO was characterized by the presence of the monoterpene hydrocarbon: α-pinene (80.4%), camphene (1.8%), β-pinene, α-phellandrene (2.8%) and 3-carene (1.0%). The total ion chromatogram (TIC) of Cedar EO and the chemical composition of CEO are presented in Figure 1 and Table 1, respectively.

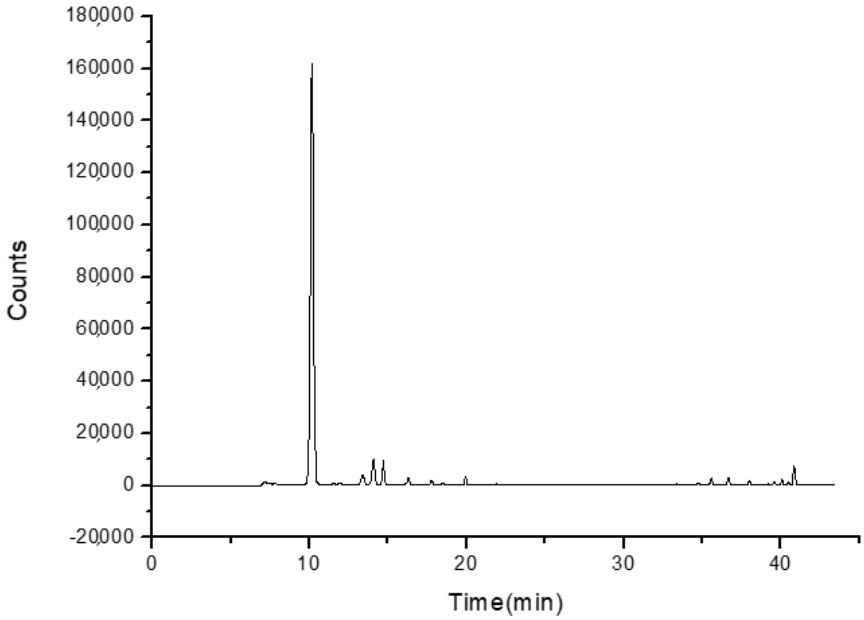

Figure 1. Total ion chromatogram (TIC) of CEO and its main components.

Table 1. Chemical composition of the CEO used in the present study.

NO.	Compound	RT	Area%
1	*α*-pinene	10.163	80.4
3	camphene	13.386	1.9
4	*β*-pinene	14.086	4.3
5	*α*-phellandrene	14.705	2.9
6	*δ*-3-carene	16.294	1.0
7	*D*-limonene	17.772	0.6
8	unidentified	40.841	2.1

3.2. Characterization of the β-CD–CEO ICs

3.2.1. Inclusion Efficiency of the β-CD–CEO ICs and Process Yield

The inclusion efficiency (IE) is one of the most critical parameters for estimating the feasibility of the encapsulation process. The obtained values presented in Table 2 were reproducible and in accordance with the ones reported in the literature for other EOs [29], suggesting the efficient encapsulation of CEO in β-CD. Several factors may affect the IE, such as the composition and concentration of the EO, the type of process used to dry the formed ICs, the type of solvent used to extract the EO from the β-CD cavity, etc. [38]. In the current work, the effect of the mass ratio of β-CD: EO on IE was investigated. The results revealed that an increase in the initial amount of β-CD (from 70:30 to 85:15 (*w*/*w*) mass ratios) in the solution led to higher IE values (up to 27%), while a further increase in β-CD (90:10 (*w*/*w*)) reduced % IE (21%). The same trend was also observed for process yield values which were satisfactory in all cases (Table 2).

Table 2. Process yield (%) and Inclusion efficiency (% IE) of the different β-CD–CEO ICs.

β-CD:CEO (*w*/*w*)	Process Yield (%)	IE (%)
90:10	69	21
85:15	78	27
80:20	72	24
70:30	65	10

3.2.2. Size, Size Distribution and Zeta-Potential

Particle size and polydispersity index (PDI) are significant findings for the characterization of ICs since they affect their physicochemical and biological properties in the final applications [39]. In the current system, the results concerning the size and size distribution, along with the zeta potential values of the formed ICs, are presented in Table 3. All prepared ICs showed a size between 315.9 nm and 769.6 nm and PDI values between 0.326 and 0.604, indicating moderate size dispersion. The particle size was found to increase with the increase in the initial amount of β-CD, which along with the PDI values, could be attributed to the strong tendency of the β-CD ICs to agglomerate because of their self-assembly in aqueous solutions [40]. As shown in Table 3, the ICs presented negative zeta potential values, between −17.5 mV and −37.0 mV, revealing the formation of stable ICs dispersion. It is generally recognized that an absolute value of zeta potential around 30 mV indicates an electrostatically stabilized suspension [41]. The β-CD–CEO IC prepared by using β-CD:CEO 80:20 (*w*/*w*) presented the most desirable size, PDI and zeta-potential values, which, in combination with the satisfactory process yield and inclusion efficiency, render it as the optimal system for further characterization and acetylcholinesterase activity studies.

Table 3. Size, polydispersity index and zeta-potential average values of the formed β-CD–CEO ICs.

β-CD:CEO (*w*/*w*)	Size (nm)	Polydispersity Index (PDI)	Zeta-Potential (mV)
90:10	769.6 ± 41.8	0.604 ± 0.066	−37.0 ± 1.8
85:15	478.6 ± 81.2	0.582 ± 0.210	−23.5 ± 0.7
80:20	403.5 ± 31.8	0.326 ± 0.037	−26.9 ± 0.9
70:30	315.9 ± 31.3	0.404 ± 0.036	−17.5 ± 2.0

3.2.3. Thermal Properties

Thermal analysis was further conducted to investigate the thermal properties of the prepared ICs and to confirm their formation. The DSC and TGA curves of the samples are presented in Figures 2 and 3, respectively.

Starting with the CEO, the DSC curve exhibited an endothermic peak at 132.6 °C that corresponds to the boiling point of the EO. The relevant thermal transition was also seen in its TGA curve, where the CEO weight loss starts at roughly 70 °C, reaching a maximum rate at 119.3 °C, with a residue at 20%. Considering the β-CD, its DSC curve revealed an endothermic peak at 131.1 °C due to the evaporation of water molecules located in the β-CD cavity, an observation that is also confirmed by the β-CD TGA curve, in which ca. 10% weight loss at roughly 100 °C is presented. Furthermore, the degradation temperature was estimated at ca. 322.1 °C, with a residue at 17.7%.

The DSC thermogram of β-CD–CEO ICs did not present the endothermic peaks owed to the CEO boiling point or to water evaporation. The DSC curve was found to be slightly different compared to the respective one of the β-CD, indicating the ICs formation. This finding ties well with our previous study [29], in which the endothermic peak of the boiling point of oregano essential oil was absent as well. In addition, the corresponding TGA curve was also found slightly different compared to the respective one of the β-CD, with the degradation temperature of β-CD–CEO ICs being estimated at ca. 319.2 °C. A weight loss at 100 °C was not observed, potentially due to the partial displacement of the water molecules in the β-CD hydrophobic cavity by the guest CEO. No significant weight loss is observed in the range of 70–120 °C, where the cedar EO loss occurs, suggesting the protection of the CEO in the β-CD cavity.

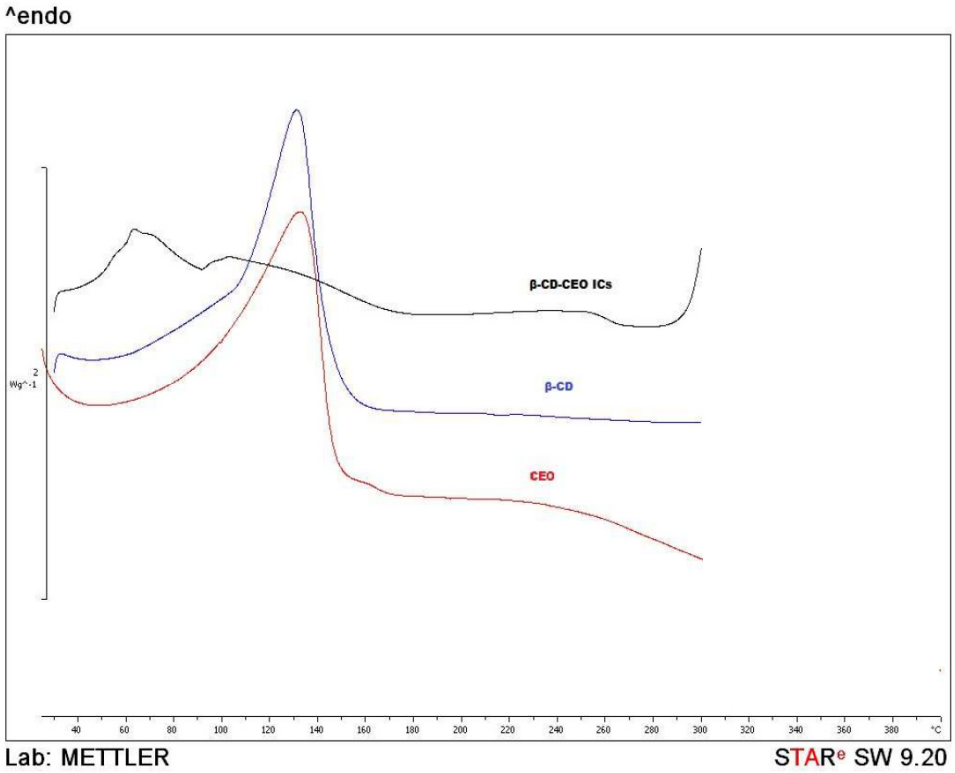

Figure 2. The comparative DSC graphs of the β-CD–CEO ICs, β-CD and CEO, heated from 30 °C to 300 °C, at a heating rate of 10 °C/min under nitrogen gas flow (20 mL/min).

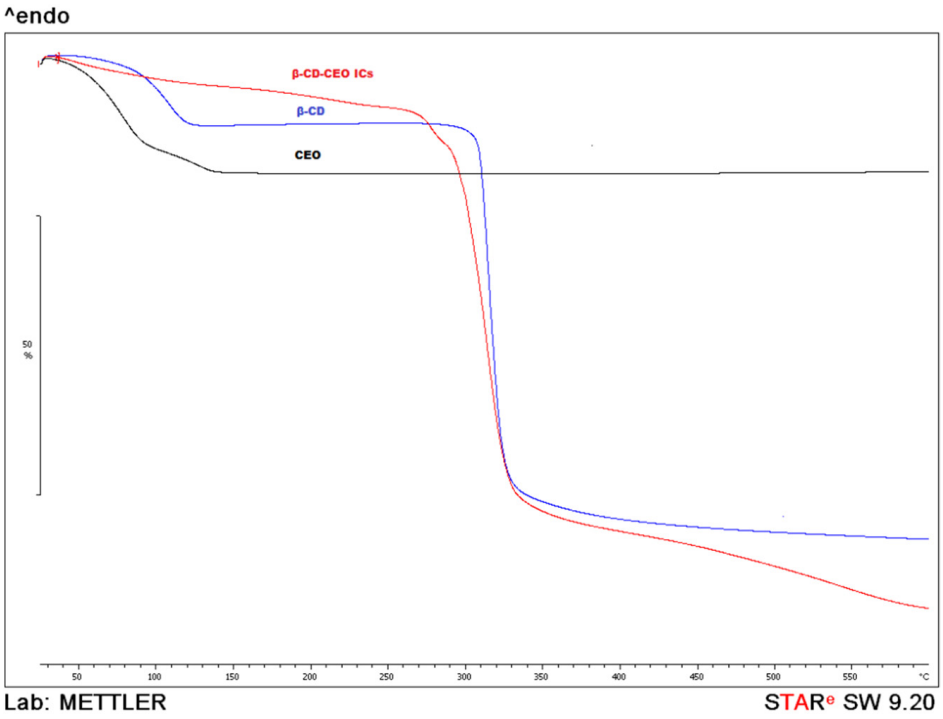

Figure 3. The comparative TGA graphs of the β-CD–CEO ICs, β-CD and CEO, heated from 25 °C to 600 °C, at a heating rate of 10 °C/min under nitrogen gas flow (10 mL/min).

3.2.4. FT-IR Analysis

This analysis was applied to acquire an insight into the interaction between the encapsulated CEO and β-CD by obtaining the FTIR spectra of the β-CD, CEO and β-CD–CEO ICs (Figure 4).

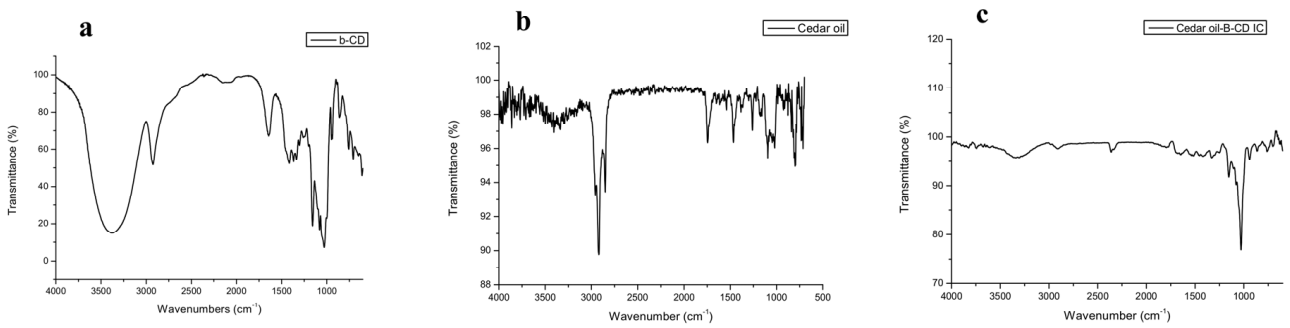

Figure 4. FT-IR spectra of: (**a**) β-CD, (**b**) CEO and (**c**) β-CD–CEO ICs in the scanning range of 500–4000 cm^{-1}.

In the FT-IR spectrum of β-CD (Figure 4a), the characteristic absorption bands were the band at 3292.35 cm^{-1} attributed to the –OH stretching vibration, the band at 2924.63 cm^{-1} attributed to the C–H stretching vibration, the band at 1643.67 cm^{-1} due to the asymmetric C–H stretching of $–CH_2$ and the band at 1414.33 cm^{-1} owing to the O–H bending vibration. Additionally, the absorption at 1020.75 cm^{-1} is attributed to the C–O stretching vibration of the secondary alcohol groups that are present in the β-CD molecule.

The major characteristic absorption bands of CEO (Figure 4b) are present at 2921.63 cm^{-1} owed to the C–H stretching vibration, at 1469.49 cm^{-1} which can be attributed to the C–C stretching vibration. The characteristic band of the C–H bending vibration appears at 808.03 cm^{-1}. The band at 794.53 cm^{-1} is attributed to the C–H out-of-plane stretching vibration of C=C–H.

In the FT-IR spectrum of β-CD–CEO ICs (Figure 4c), the characteristic absorption bands of β-CD were shifted. Specifically, the bands that were attributed to the –OH stretching vibration and to the C–H stretching vibration appeared at 3305.98 cm^{-1} and 1639.02 cm^{-1}, respectively; thus, they were shifted by 13.63 cm^{-1} and 4.65 cm^{-1}. Small shifts were also observed for the absorption bands owed to the O–H bending and C–O stretching vibrations (2.6 and 1.4 cm^{-1}, respectively) (Table 4).

Table 4. Major characteristic absorption bands of β-CD and β-CD–CEO ICs.

	–OH Stretching	**C–H Stretching**	**C–H Asymmetric Stretching of CH_2**	**C–C Stretching Vibration**	**O–H Bending**	**C–O Stretching of Secondary Alcohols**
CEO	-	2921.63	-	1469.49	-	-
β-CD	3292.35	2924.63	1643.67	-	1414.33	1020.75
β-CD–CEO ICs	3305.98	2909.09	1639.02	-	1411.73	1022.15

The absence of the characteristic bands of CEO in the FT-IR spectrum of ICs, combined with the shifted characteristic bands of β-CD, confirms the encapsulation of CEO in the β-CD ICs and proves the formation of inclusion complexes.

3.2.5. NMR Analysis

^{1}H NMR analysis of β-CD and β-CD–CEO IC was performed at 300 MHz in D_2O, while the ^{1}H NMR spectrum of the pure CEO was obtained at 300 MHz in DMSO-d_6. In the CEO NMR spectrum, in the range of 1.63 ppm to 0.82 ppm, the methyl groups of

the different CEO terpenoids were observed, while the peaks at 1.63 ppm, 1.26 ppm and 0.82 ppm could be attributed to the methyl groups of alpha-pinene (the main constituent). Different peaks of lower intensity were also presented in the range of 2.36 ppm to 1.90 ppm attributed to the protons of the bicyclic system of alpha-pinene, as well as of the different terpenoids contained in CEO (Figure 5).

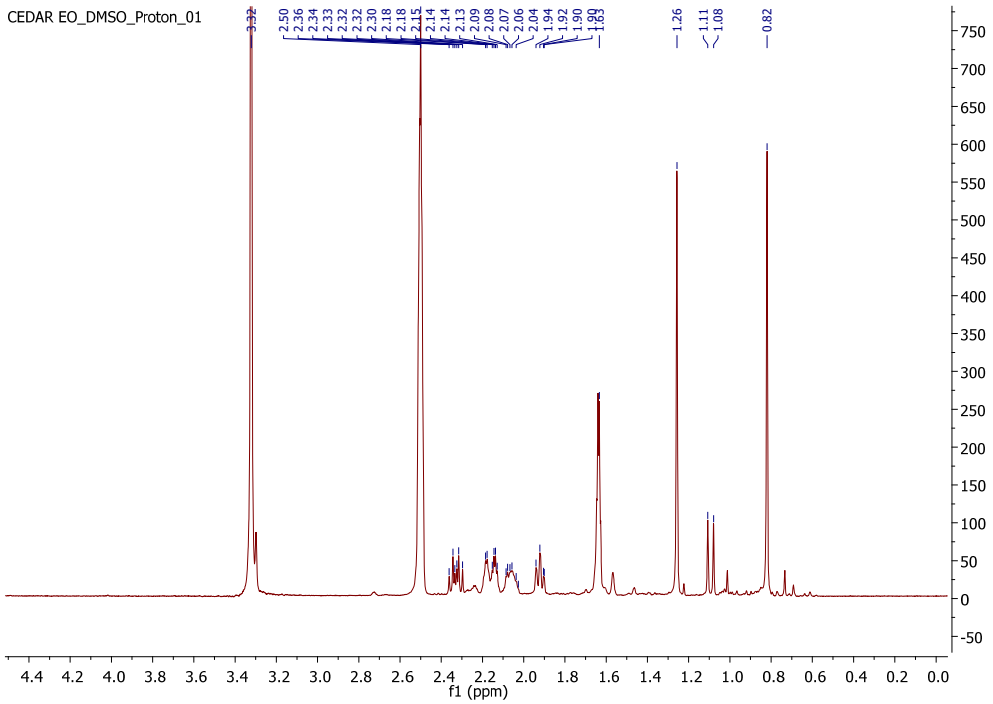

Figure 5. ^{1}H NMR spectrum (300 MHz, DMSO-d_6) of the CEO.

The encapsulation of CEO into the β-CD cavity is evidenced by the chemical shift changes observed in the ^{1}H-NMR spectra of both β-CD and the IC, as shown in Figure 6. The chemical shifts of protons H-3 and H-5 of β-CD are particularly important since these protons are located inside the hydrophobic cavity [42]. The $\Delta\delta$ values of NMR signals of β-CD before and after the formation of the ICs are presented in Table 5. The highest chemical shift changes were observed for H-5 (−0.015 ppm) and H-3 (−0.011 ppm), whereas for the remaining β-CD protons, no noteworthy changes were detected. These upfield shifts along with the presence of the signal due to the protons of the methyl groups of a-pinene, the main constituent of the cedar essential oil, and the absence of the peaks presented in the range of 2.36 ppm to 1.90 ppm reveal the entrapment of the bicyclic system of alpha-pinene in the β-CD cavity and the successful formation of the inclusion complex.

3.3. Phase Solubility Studies

The phase solubility diagram of cedar essential oil with β-CD at 37 °C is illustrated in Figure 7. The diagram shows a linear trend with a slope < 1. According to Higuchi and Connors (1965), diagrams exhibiting a linear relationship are considered A_L-type. The solubility of cedar essential oil increases linearly as a function of β-CD concentration (0–10 mmol/L). More specifically, the initial solubility was found at 1.03 g/L at 37 °C and increased to 5.55 g/L in the presence of 10 mmol/L of β-CD. These results showed that β-CD could enhance the aqueous solubility of cedar essential oil.

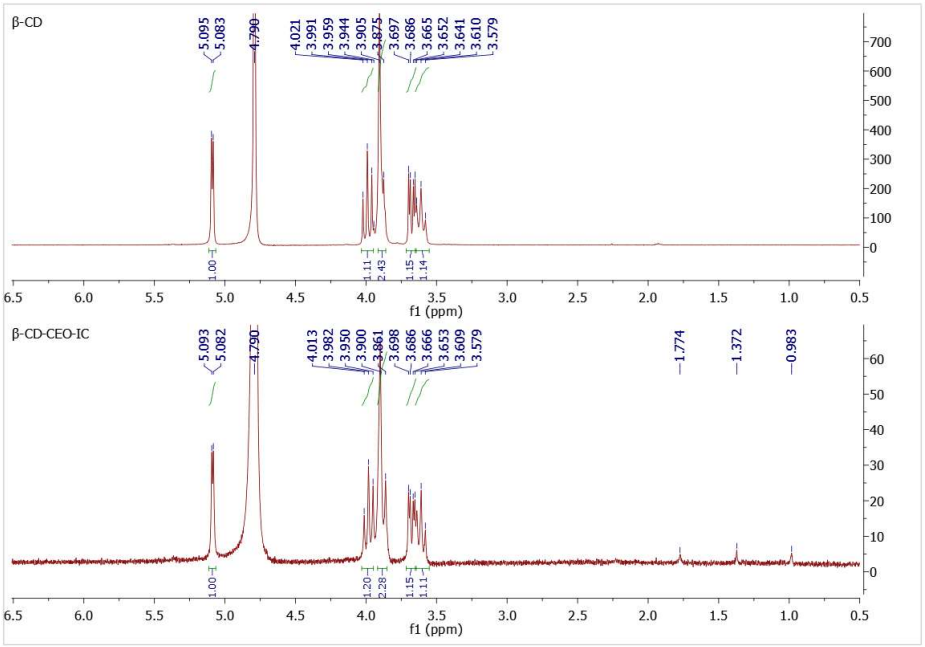

Figure 6. ^{1}H NMR spectra (300 MHz, D_2O) of β-CD and β-CD–CEO IC in the region of 6.5 to 0.5 ppm.

Table 5. Chemical shift changes of ^{1}H-NMR signals of β-CD and β-CD–CEO ICs.

Proton	Chemical Shifts (δ_1) of β-CD Protons (ppm)	Chemical Shifts (δ_2) of β-CD Protons in β-CD–CEO ICs (ppm)	$\Delta\delta = \delta_2 - \delta_1$ (ppm)
H-1	5.091	5.087	−0.004
H-2	3.676	3.675	−0.001
H-3	3.992	3.981	−0.011
H-4	3.610	3608	−0.002
H-5	3.875	3.860	−0.015
H-6	3.905	3.898	−0.007

3.4. In Vitro Release Study of the β-CD–Cedar Essential Oil (CEO) ICs

The in vitro release study of the β-CD–Cedar Essential Oil (CEO) ICs was performed in phosphate-buffered solution (pH 7.4) at 37 °C. The release of cedar essential oil from β-CD ICs at 37 °C is illustrated in Figure 8. The release profile was biphasic, with an initial burst release of 75% during the first 5 h. This was followed by a gradual release, while the cumulative release percentage reached 89% after 24 h. Therefore, the formed inclusion complex might be a potential sustained delivery release system for cedar essential oil.

The release data were analyzed by kinetic studies according to zero order, first order, second order, Higuchi and Korsmeyer–Peppas models. Comparing the R^2 values for the different kinetic models, it was found that the in vitro release of the CEO was better explained by non-Fickian diffusion (anomalous transport) compared to Fickian diffusion. The results from the kinetics of cedar EO release for different models are given in Table 6. The release kinetics better fitted on the Higuchi model and the corresponding curve along with Korsmeyer–Peppas curve are shown in Figures 9 and 10, respectively.

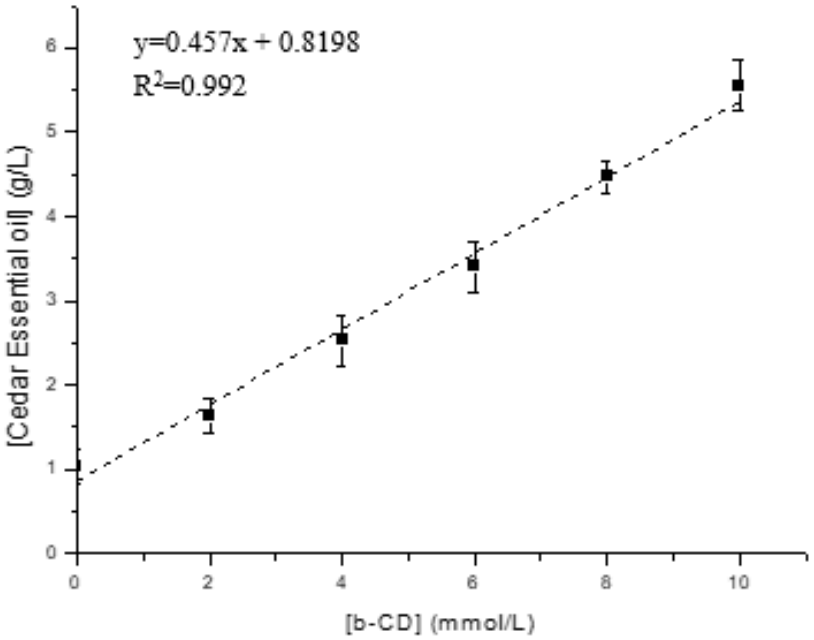

Figure 7. Phase solubility curve of cedar essential oil with β-CD at 37 °C.

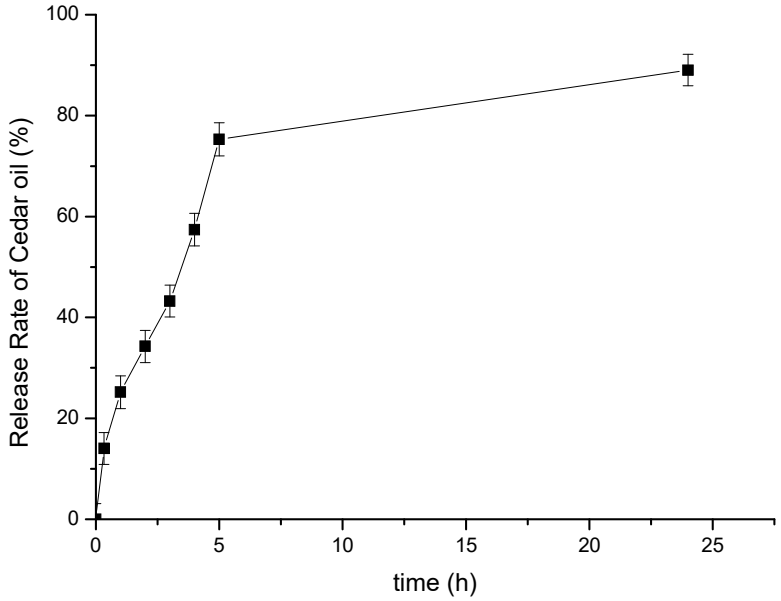

Figure 8. Cumulative release of Cedar Essential Oil (CEO) from β-CD-CEO ICs at pH 7.4 and at 37 ± 0.5 °C.

Table 6. Results from kinetics of drug release for different models.

Kinetic Model	R^2	Equation
Zero order	0.605	y = 2.9846x + 27.641
First order	0.2507	y = 0.0397x + 1.2179
Higuchi	0.8491	y = 18.893x + 9.5919
Korsmeyer-Peppas	0.9502	y = 0.6455x + 0.1683

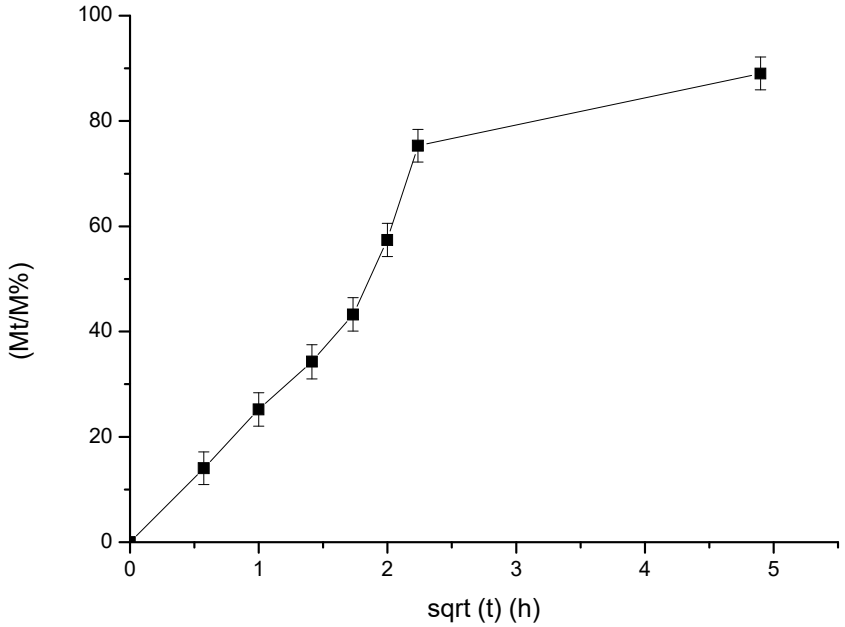

Figure 9. Cumulative percentage release vs. square root of time in hours.

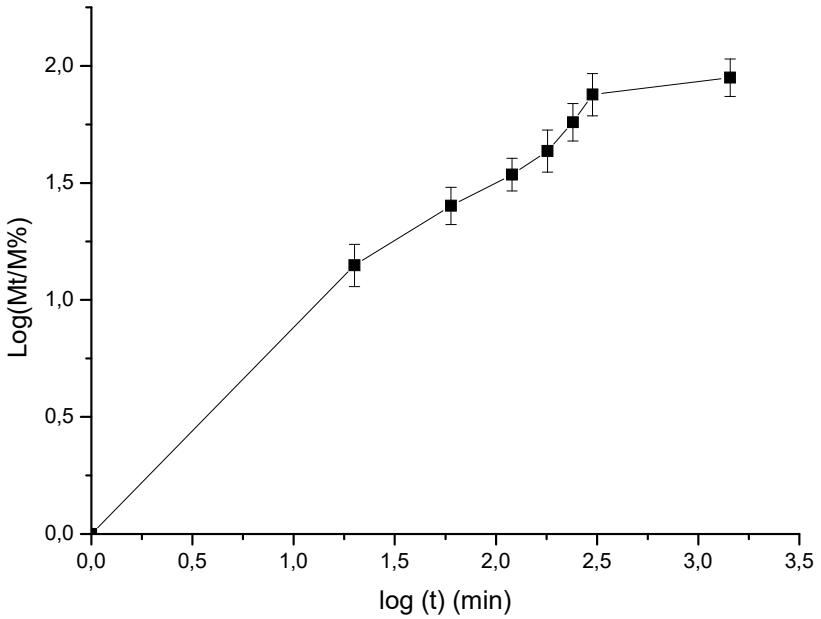

Figure 10. Logarithm of cumulative percentage release vs. logarithm of time in minutes.

3.5. Acetylcholinesterase (AChE) Inhibitory Activity

For the in vitro acetylcholinesterase inhibition assay, AChE from *electrophorus electricus* was used due to its homology to the human acetylcholinesterase [43]. CEO was tested for its ability to inhibit acetylcholinesterase in vitro in a concentration range of 120–20 µg/mL in DMSO, and IC_{50} was calculated as 37 µg/mL (Table 7).

Table 7. AChE inhibitory capacity of the tested samples.

Sample	IC_{50} (μg/mL)			
β-cyclodextrin (β-CD)	No activity			
Cedar Essential Oil (CEO)	37			
β-CD–CEO ICs (H_2O)	t = 0	t = 2 h	t = 5 h	t = 24 h
	No activity	No activity	76.8	60.8
β-CD–CEO ICs (DMSO)	t = 0	t = 2 h	t = 5 h	
	85.3	66.8	65.4	
Galantamine	0.34			

EO's composition and biological activities are significantly affected by the place of origin, the extraction method etc. For instance, *Juniperus phoenicea* cultivated in Portugal and extracted using a hydroethanolic solution from the leaves of the plant exhibited 50% AChE inhibition at a concentration of 400 μg/mL approximately [44]. Moreover, the CEO extracted from the aerial parts of the plant by hydrodistillation and collected from Algeria, containing mostly α-pinene (over 41.8%), followed by δ-3-carene (8.4%), exhibited 40% AChE inhibition at a concentration of 1 mg/mL [45]. However, similar inhibition (34%) was obtained at only 20 μg/mL in the present research (Figure 11).

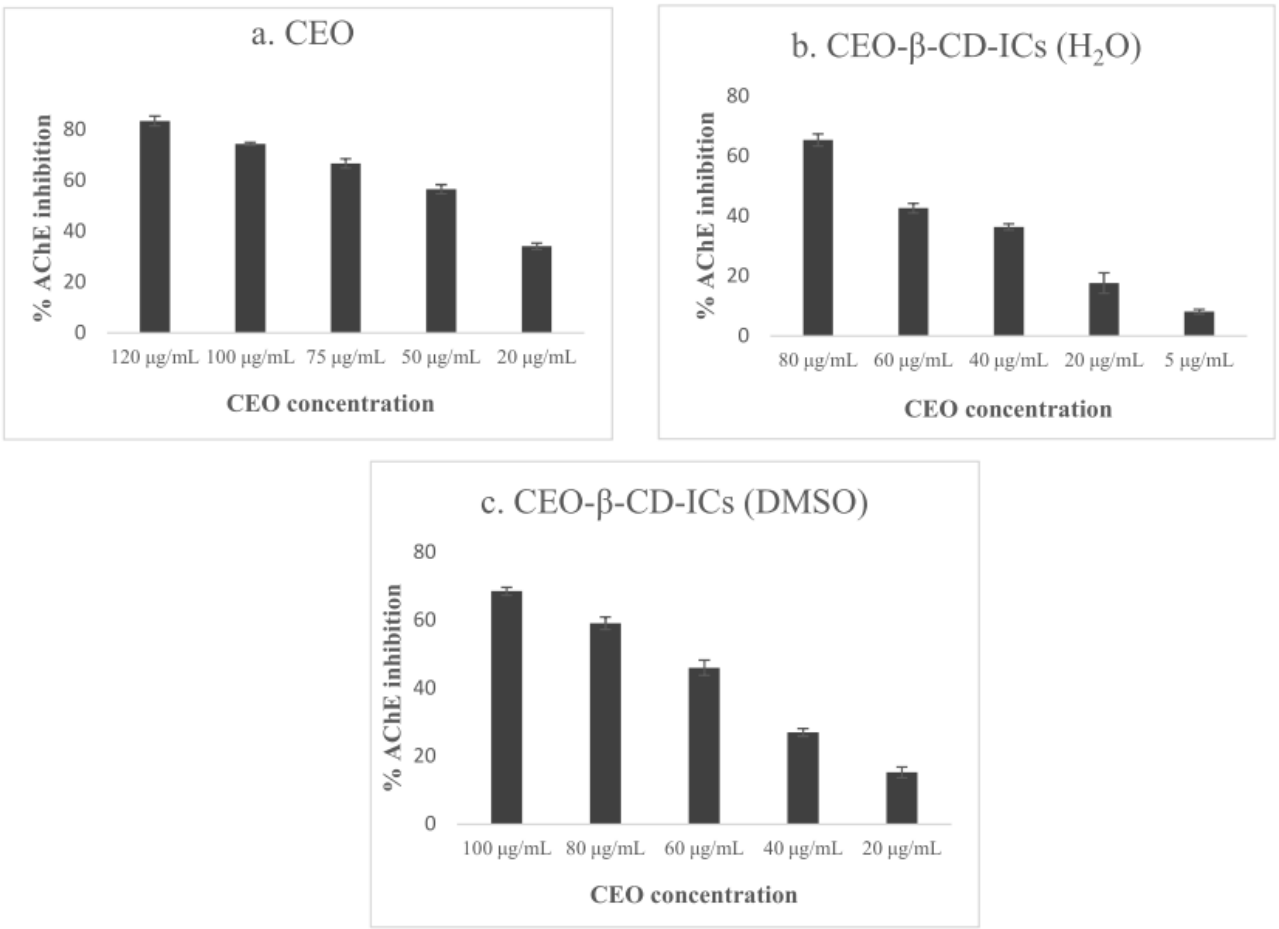

Figure 11. Effect of (**a**) CEO, (**b**) CEO-β-CD ICs dispersed in H_2O at t = 24 h and (**c**) CEO-β-CD ICs dispersed in DMSO at t = 5 h on AChE inhibition.

As far as the inclusion complexes are concerned, β-CD–CEO ICs dispersed in DMSO exhibited an IC_{50} of 85.3 μg/mL at t = 0, which however was gradually improved, reaching an IC_{50} value of approximately 65 μg/mL at t = 2 h and t = 5 h (Table 7). On the other hand, β-CD–CEO ICs dispersed in water were not able to inhibit AChE effectively at t = 0 or t = 2 h, which is in accordance with the release study, indicating approximately 14% and 34% cumulative release at t = 15 min and t = 2 h, respectively. However, at t = 5 h, the ICs exhibited an IC_{50} of 76.8 μg/mL, and at t = 24 h, an IC_{50} of 60.8 μg/mL, indicating the sustained and partial release of the EO from the inclusion complex and the improvement of the biological response. Free β-CD does not possess any AChE inhibitory capacity.

The results reveal that β-CD–CEO ICs dispersed in DMSO presented IC_{50} 65.4 μg/mL at t = 5 h, while β-CD–CEO ICs dispersed in ultra-pure water showed similar inhibitory activity at t = 24 h (IC_{50} 60.8 μg/mL), indicating the increased solubility and the gradual release of CEO in an aqueous solution as well as its prolonged bioactivity. The results are displayed in Table 7 and Figure 11.

4. Conclusions

The current research demonstrated the efficient encapsulation of *Juniperus phoenicea* essential oil in β-cyclodextrin using the co-precipitation method. CEO was successfully encapsulated in β-CD with process yield and inclusion efficiency values reaching up to 78% and 27%, respectively. The mean diameter of ICs ranged between 315.9 nm and 769.6 nm, with anionic zeta potentials. The results from the analytical techniques confirmed the successful encapsulation of CEO in β-CD and the formation of ICs. The in vitro release of CEO from the β-CD–CEO ICs indicated a controlled diffusion release in a biphasic profile, which could be expressed well by the Higuchi equation: $Q = 18.893\ t^{1/2} + 9.5919$, $R^2 = 0.8491$. The studied CEO exhibited potent AChE inhibitory activity (IC_{50} 37 μg/mL) in vitro, while β-CD–CEO ICs were found to significantly inhibit AChE as well (IC_{50} 65.4 and 60.8 μg/mL in DMSO and H_2O, respectively). The AChE inhibitory activity of β-CD–CEO ICs was examined both in DMSO and in an aqueous medium, which is essential for its use in industrial applications (e.g., pharmaceutics or cosmetics). The results of this research provide evidence that the formation of inclusion complexes of CEO with β-CD promotes the aqueous solubility of CEO and prolongs the AChE inhibitory activity even at aqueous medium; thus, it is an advantageous approach for the exploitation of this essential oil.

Author Contributions: Conceptualization, A.D.; data curation, E.K., I.P., A.K., G.P. and A.A.; methodology, E.K., I.P., A.K. and G.P.; project administration, A.D; resources, A.D.; supervision, A.D.; writing—original draft preparation, E.K., I.P., A.K., G.P., S.G. and A.D.; writing—review and editing, E.K. and A.D. All authors have read and agreed to the published version of the manuscript.

Funding: This research is co-financed by Greece and the European Union (ESF) through the Operational Programme (Human Resources Development, Education and Lifelong Learning) in the context of the project "Strengthening Human Resources Research Potential via Doctorate Research" (MIS-5000432), implemented by the State Scholarships Foundation (ΙΚΥ).

Institutional Review Board Statement: Not applicable.

Informed Consent Statement: Not applicable.

Data Availability Statement: All data generated or analyzed during this study are included in this published article.

Acknowledgments: I.P. would like to acknowledge financial support from the Leventis Foundation (scholarship for PhD studies). A.K. gratefully acknowledges State Scholarships Foundation (ΙΚΥ).

Conflicts of Interest: The authors declare that they have no competing interests.

References

1. Risaliti, L.; Kehagia, A.; Daoultzi, E.; Lazari, D.; Bergonzi, M.C.; Vergkizi-Nikolakaki, S.; Hadjipavlou-Litina, D.; Bilia, A.R. Liposomes loaded with Salvia triloba and Rosmarinus officinalis essential oils: In vitro assessment of antioxidant, antiinflammatory and antibacterial activities. *J. Drug Deliv. Sci. Technol.* **2019**, *51*, 493–498. [CrossRef]
2. Douros, A.; Hadjipavlou-Litina, D.; Nikolaou, K.; Skaltsa, H. The occurrence of flavonoids and related compounds in Cedrus brevifolia A. Henry ex Elwes & A. Henry needles. inhibitory potencies on lipoxygenase, linoleic acid lipid peroxidation and antioxidant activity. *Plants* **2017**, *7*, 1. [CrossRef]
3. Brochot, A.; Guilbot, A.; Haddioui, L.; Roques, C. Antibacterial, antifungal, and antiviral effects of three essential oil blends. *Microbiologyopen* **2017**, *6*, e00459. [CrossRef]
4. Fitsiou, E.; Pappa, A. Anticancer activity of essential oils and other extracts from aromatic plants grown in Greece. *Antioxidants* **2019**, *8*, 290. [CrossRef]
5. Qneibi, M.; Jaradat, N.; Hawash, M.; Zaid, A.N.; Natsheh, A.-R.; Yousef, R.; Abuhasan, Q. The neuroprotective role of *Origanum syriacum* L. and *Lavandula dentata* L. Essential oils through their effects on AMPA receptors. *BioMed Res. Int.* **2019**, *2019*, 5640173. [CrossRef]
6. Jugreet, B.S.; Suroowan, S.; Rengasamy, R.K.; Mahomoodally, M.F. Chemistry, bioactivities, mode of action and industrial applications of essential oils. *Trends Food Sci. Technol.* **2020**, *101*, 89–105. [CrossRef]
7. Eslahi, H.; Fahimi, N.; Sardarian, A.R. Chemical Composition of Essential Oils. In *Essential Oils in Food Processing*; Wiley: New York, NY, USA, 2017; pp. 119–171.
8. Wang, H.-F.; Yih, K.-H.; Yang, C.-H.; Huang, K.-F. Anti-oxidant activity and major chemical component analyses of twenty-six commercially available essential oils. *J. Food Drug Anal.* **2017**, *25*, 881–889. [CrossRef] [PubMed]
9. Leporini, M.; Bonesi, M.; Loizzo, M.R.; Passalacqua, N.G.; Tundis, R. The essential oil of salvia *rosmarinus* spenn. From Italy as a source of health-promoting compounds: Chemical profile and antioxidant and cholinesterase inhibitory activity. *Plants* **2020**, *9*, 798. [CrossRef]
10. Zhu, S.; Li, H.; Dong, J.; Yang, W.; Liu, T.; Wang, Y.; Wang, X.; Wang, M.; Zhi, D. Rose Essential Oil Delayed Alzheimer's Disease-Like Symptoms by SKN-1 Pathway in C. elegans. *J. Agric. Food Chem.* **2017**, *65*, 8855–8865. [CrossRef]
11. Bittner, E.A.; Martyn, J.J. Neuromuscular physiology and pharmacology. In *Pharmacology and Physiology for Anesthesia:Foundations and Clinical Application*; Elsevier: Amsterdam, The Netherlands, 2019; pp. 412–427.
12. García-Ayllón, M.-S.; Small, D.H.; Avila, J.; Saez-Valero, J. Revisiting the role of acetylcholinesterase in Alzheimer's disease: Cross-talk with P-tau and β-amyloid. *Front. Mol. Neurosci.* **2011**, *4*, 22. [CrossRef]
13. Dos Santos, T.C.; Gomes, T.M.; Pinto, B.A.S.; Camara, A.L.; Paes, A.M.D.A. Naturally occurring acetylcholinesterase inhibitors and their potential use for Alzheimer's disease therapy. *Front. Pharmacol.* **2018**, *9*, 1192. [CrossRef]
14. Patil, D.N.; Patil, S.A.; Sistla, S.; Jadhav, J.P. Comparative biophysical characterization: A screening tool for acetylcholinesterase inhibitors. *PLoS ONE* **2019**, *14*, e0215291. [CrossRef] [PubMed]
15. Mazur, M.; Klajbor, K.; Kielich, M. Intra-specific differentiation of Juniperus phoenicea in the western Mediter-ranean region revealed in morphological multivariate analysis. *Dendrobiology* **2010**, *63*, 21–31.
16. Ennajar, M.; Bouajila, J.; Lebrihi, A.; Mathieu, F.; Abderraba, M.; Raies, A.; Romdhane, M. Chemical Composition and Antimicrobial and Antioxidant Activities of Essential Oils and Various Extracts of *Juniperus phoenicea* L. (Cupressacees). *J. Food Sci.* **2009**, *74*, M364–M371. [CrossRef]
17. Ait-Ouazzou, A.; Lorán, S.; Arakrak, A.; Laglaoui, A.; Rota, C.; Herrera, A.; Pagán, R.; Conchello, P. Evaluation of the chemical composition and antimicrobial activity of Mentha pulegium, Juniperus phoenicea, and Cyperus longus essential oils from Morocco. *Food Res. Int.* **2012**, *45*, 313–319. [CrossRef]
18. El Jemli, M.; Kamal, R.; Marmouzi, I.; Zerrouki, A.; Cherrah, Y.; Alaoui, K. Radical-Scavenging activity and ferric reducing ability of *Juniperus thurifera* (L.), *J. Oxycedrus* (L.), *J. Phoenicea* (L.) and *Tetraclinis articulata* (L.). *Adv. Pharmacol. Sci.* **2016**, *2016*, 6392656. [CrossRef]
19. Bouassida, K.Z.; Makni, S.; Tounsi, A.; Jlaiel, L.; Trigui, M.; Tounsi, S. Effects of Juniperus phoenicea Hydroalcoholic Extract on Inflammatory Mediators and Oxidative Stress Markers in Carrageenan-Induced Paw Oedema in Mice. *BioMed Res. Int.* **2018**, *2018*, 3785487. [CrossRef]
20. Öztürk, M.; Tümen, I.; Uğur, A.; Aydoğmuş-Öztürk, F.; Topçu, G. Evaluation of fruit extracts of six Turkish Juniperus species for their antioxidant, anticholinesterase and antimicrobial activities. *J. Sci. Food Agric.* **2011**, *91*, 867–876. [CrossRef]
21. Kfoury, M.; Landy, D.; Fourmentin, S. Characterization of cyclodextrin/volatile inclusion complexes: A review. *Molecules* **2018**, *23*, 1204. [CrossRef]
22. Detsi, A.; Kavetsou, E.; Kostopoulou, I.; Pitterou, I.; Pontillo, A.R.N.; Tzani, A.; Christodoulou, P.; Siliachli, A.; Zoumpoulakis, P. Nanosystems for the Encapsulation of Natural Products: The case of chitosan biopolymer as a matrix. *Pharmaceutics* **2020**, *12*, 669. [CrossRef] [PubMed]
23. Majeed, H.; Bian, Y.-Y.; Ali, B.; Jamil, A.; Majeed, U.; Khan, Q.F.; Iqbal, K.J.; Shoemaker, C.F.; Fang, Z. Essential oil encapsulations: Uses, procedures, and trends. *RSC Adv.* **2015**, *5*, 58449–58463. [CrossRef]
24. Maes, C.; Bouquillon, S.; Fauconnier, M.-L. Encapsulation of essential oils for the development of biosourced pesticides with controlled release: A review. *Molecules* **2019**, *24*, 2539. [CrossRef]

25. Ben, J.M.; Falleh, H.; Ksouri, R. Encapsulation of Natural Bioactive Compounds: Nanoemulsion Formulation to Enhance Essential Oils Activities. In *Microencapsulation–Processes, Technologies and Industrial Applications*; IntechOpen: London, UK, 2019.
26. Wadhwa, G.; Kumar, S.; Chhabra, L.; Mahant, S.; Rao, R. Essential oil–cyclodextrin complexes: An updated review. *J. Incl. Phenom. Macrocycl. Chem.* **2017**, *89*, 39–58. [CrossRef]
27. Jambhekar, S.S.; Breen, P. Cyclodextrins in pharmaceutical formulations I: Structure and physicochemical properties, formation of complexes, and types of complex. *Drug Discov. Today* **2016**, *21*, 356–362. [CrossRef]
28. Jansook, P.; Ogawa, N.; Loftsson, T. Cyclodextrins: Structure, physicochemical properties and pharmaceutical applications. *Int. J. Pharm.* **2018**, *535*, 272–284. [CrossRef]
29. Kotronia, M.; Kavetsou, E.; Loupassaki, S.; Kikionis, S.; Vouyiouka, S.; Detsi, A. Encapsulation of Oregano (*Origanum onites* L.) Essential Oil in β-Cyclodextrin (β-CD): Synthesis and Characterization of the Inclusion Complexes. *Bioengineering* **2017**, *4*, 74. [CrossRef] [PubMed]
30. Ren, X.; Yue, S.; Xiang, H.; Xie, M. Inclusion complexes of eucalyptus essential oil with β-cyclodextrin: Preparation, characterization and controlled release. *J. Porous Mater.* **2018**, *25*, 1577–1586. [CrossRef]
31. Nait, B.Y.; Nait, B.R.; Hadj-Ziane-Zafour, A. Nanodispersions stabilized by β-cyclodextrin nanosponges: Application for simultaneous enhancement of bioactivity and stability of sage essential oil. *Drug Dev. Ind. Pharm.* **2019**, *45*, 333–347. [CrossRef] [PubMed]
32. Santos, E.H.; Kamimura, J.A.; Hill, L.E.; Gomes, C.L. Characterization of carvacrol beta-cyclodextrin inclusion complexes as delivery systems for antibacterial and antioxidant applications. *LWT-Food Sci. Technol.* **2015**, *60*, 583–592. [CrossRef]
33. Kfoury, M.; Pipkin, J.; Antle, V.; Fourmentin, S. Captisol®: An efficient carrier and solubilizing agent for essential oils and their components. *Flavour Fragr. J.* **2017**, *32*, 340–346. [CrossRef]
34. Saokham, P.; Muankaew, C.; Jansook, P.; Loftsson, T. Solubility of cyclodextrins and drug/cyclodextrin complexes. *Molecules* **2018**, *23*, 1161. [CrossRef]
35. Mircioiu, C.; Voicu, V.; Anuta, V.; Tudose, A.; Celia, C.; Paolino, D.; Fresta, M.; Sandulovici, R.; Mircioiu, I. Mathematical modeling of release kinetics from supramolecular drug delivery systems. *Pharmaceutics* **2019**, *11*, 140. [CrossRef]
36. Hasnat, A.; Pervin, M.; Lim, B.O. Acetylcholinesterase inhibition and in vitro and in vivo antioxidant activities of ganoderma lucidum grown on germinated brown rice. *Molecules* **2013**, *18*, 6663–6678. [CrossRef]
37. Ellman, G.L.; Courtney, K.D.; Andres, V., Jr.; Featherstone, R.M. A new and rapid colorimetric determination of acetylcholinesterase activity. *Biochem. Pharmacol.* **1961**, *7*, 88–95. [CrossRef]
38. Da Rocha, N.A.C.; de Oliveira da Rocha, A.B.; Maraschin, M.; Di Piero, R.M.; Almenar, E. Factors affecting the entrapment efficiency of β-cyclodextrins and their effects on the formation of inclusion complexes containing essential oils. *Food Hydrocoll.* **2018**, *77*, 509–523. [CrossRef]
39. Kesente, M.; Kavetsou, E.; Roussaki, M.; Blidi, S.; Loupassaki, S.; Chanioti, S.; Siamandoura, P.; Stamatogianni, C.; Philippou, E.; Papaspyrides, C.; et al. Encapsulation of olive leaves extracts in biodegradable PLA nanoparticles for use in cosmetic formulation. *Bioengineering* **2017**, *4*, 75. [CrossRef] [PubMed]
40. Hill, L.E.; Gomes, C.; Taylor, T.M. Characterization of beta-cyclodextrin inclusion complexes containing essential oils (trans-cinnamaldehyde, eugenol, cinnamon bark, and clove bud extracts) for antimicrobial delivery applications. *LWT-Food Sci. Technol.* **2013**, *51*, 86–93. [CrossRef]
41. Joseph, E.; Singhvi, G. Multifunctional Nanocrystals for Cancer Therapy: A Potential Nanocarrier. In *Nanomaterials for Drug Delivery and Therapy*; Elsevier: Amsterdam, The Netherlands, 2019; ISBN 9780128165058.
42. Saha, S.; Roy, A.; Roy, K.; Roy, M.N. Study to explore the mechanism to form inclusion complexes of β-cyclodextrin with vitamin molecules. *Sci. Rep.* **2016**, *6*, 35764. [CrossRef]
43. Chainoglou, E.; Siskos, A.; Pontiki, E.; Hadjipavlou-Litina, D. Hybridization of Curcumin Analogues with Cinnamic Acid Derivatives as Multi-Target Agents Against Alzheimer's Disease Targets. *Molecules* **2020**, *25*, 4958. [CrossRef] [PubMed]
44. Tavares, L.; McDougall, G.J.; Fortalezas, S.; Stewart, D.; Ferreira, R.B.; Santos, C.N. The neuroprotective potential of phenolic-enriched fractions from four Juniperus species found in Portugal. *Food Chem.* **2012**, *135*, 562–570. [CrossRef]
45. Cheraif, K.; Bakchiche, B.; Gherib, A.; Bardaweel, S.K.; Çol Ayvaz, M.; Flamini, G.; Ascrizzi, R.; Ghareeb, M.A. Chemical composition, antioxidant, anti-tyrosinase, anti-CHolinesterase and cytotoxic activities of essential oils of six Algerian plants. *Molecules* **2020**, *25*, 1710. [CrossRef] [PubMed]